Inorg. Chem. **2008**, *47*, 10090−10099

A Rational Basis for the Axial Ligand Effect in C−H Oxidation by [MnO(porphyrin)(X)]$^+$ (X = H_2O, OH^-, O^{2-}) from a DFT Study

David Balcells,[†] Christophe Raynaud,[†] Robert H. Crabtree,[‡] and Odile Eisenstein*[,†]

Institut Charles Gerhardt Montpellier, UMR 5253 CNRS-UM2-ENSCM-UM1, Université Montpellier 2, cc-1501 Place Eugène Bataillon, 34095, Montpellier, France, and Department of Chemistry, Yale University, P.O. Box 208107, New Haven, Connecticut 06520-8107

Received July 22, 2008

Oxyl radical character in the Mn═O group of the title system is shown from a density functional theory study to be essential for efficient C−H cleavage, which is a key step in C−H oxidation. Since oxyl species have elongated Mn−O bonds relative to the more usual oxo species of type Mn═O, the normal expectation would be that high trans-influence ligands X should facilitate oxyl character by elongating the Mn−O bond and thus enhance both oxyl character and reactivity. Contrary to this expectation, but in line with the experimental data (Jin, N.; Ibrahim, M.; Spiro, T. G.; Groves, J. T. *J. Am. Chem. Soc.* **2007**, *129*, 12416), we find that reactivity increases along the series X = O^{2-} < OH^- < H_2O for the following reasons. The ground-state singlet (**S**) is unreactive for all X, and only the higher-energy triplet (**T**) and quintet (**Q**) states have the oxyl character needed for reactivity, but the higher trans-influence X ligands are also shown to increase the **S**/**T** and **S**/**Q** gaps, thus making attainment of the needed **T** and **Q** states harder. The latter effect is dominant, and high trans-influence X ligands thus disfavor reaction. The higher reactivity in the presence of acid noted by Groves and co-workers is thus rationalized by the preference for having X = H_2O over OH^- or O^{2-}.

Introduction

Metal-catalyzed C−H bond oxidation has a prominent place in modern chemistry,[1] synthetic metalloporphyrins[2] being among the best known catalysts for this challenging transformation. Iron porphyrin complexes[3] are relevant to C−H hydroxylation in heme enzymes like cytochrome P450.[4] Synthetic manganese porphyrins[5] are excellent C−H hydroxylation catalysts in their own right, usually outperforming their iron analogues.[6]

Groves'[7] rebound mechanism (Scheme 1) is generally accepted for Mn,[8,9] for Fe in cytochrome P450,[10] and for a variety of Ru catalysts,[11] although alternatives have been

* Author to whom correspondence should be addressed. E-mail: odile.eisenstein@univ-montp2.fr.
[†] Université Montpellier 2.
[‡] Yale University.

(1) (a) Shilov, A. E.; Shul'pin, G. B. *Chem. Rev.* **1997**, *97*, 2879–2932. (b) Dyker, G. *Angew. Chem., Int. Ed.* **1999**, *38*, 1699–1712. (c) Labinger, J. A.; Bercaw, J. E. *Nature* **2002**, *417*, 507–514. (d) Pamplin, C. B.; Legzdins, P. *Acc. Chem. Res.* **2003**, *36*, 223–233. (e) *Activation and Functionalization of C-H Bonds*; Goldberg, K. I., Goldman, A. S. Eds.; Oxford University Press: Washington, DC, 2004. (f) Lersch, M.; Tilset, M. *Chem. Rev.* **2005**, *105*, 2471–2526. (g) Godula, K.; Sames, D. *Science* **2006**, *312*, 67–72. (h) Bergman, R. G. *Nature* **2007**, *446*, 391–393. (i) Merkx, M.; Kopp, D. A.; Sazinsky, M. H.; Blazyk, J. L.; Muller, J.; Lippard, S. J. *Angew. Chem., Int. Ed.* **2001**, *40*, 2782–2807. (j) Que, L.; Dong, Y. H. *Acc. Chem. Res.* **1996**, *29*, 190–196.
(2) (a) Williams, R. J. P. *Chem. Rev.* **1956**, *56*, 299–328. (b) Lavallee, D. K. *Coord. Chem. Rev.* **1985**, *61*, 55–96. (c) Brothers, P. J.; Collman, J. P. *Acc. Chem. Res.* **1986**, *19*, 209–215. (d) Meunier, B. *Chem. Rev.* **1992**, *92*, 1411–1456. (e) Brand, H.; Arnold, J. *Coord. Chem. Rev.* **1995**, *140*, 137–168. (f) Brothers, P. J. *Adv. Organomet. Chem.* **2001**, *46*, 223–321. (g) Che, C. M.; Huang, J. S. *Coord. Chem. Rev.* **2002**, *231*, 151–164. (h) Rose, E.; Andrioletti, B.; Zrig, S.; Quelquejeu-Ehteve, M. *Chem. Soc. Rev.* **2005**, *34*, 573–583. (i) Simonneaux, G.; Tagliatesta, P. *J. Porphyrins Phthalocyanines* **2004**, *8*, 1166–1171. (j) Woggon, W. D. *Acc. Chem. Res.* **2005**, *38*, 127–136.
(3) (a) Groves, J. T.; Haushalter, R. C.; Nakamura, M.; Nemo, T. E.; Evans, B. J. *J. Am. Chem. Soc.* **1981**, *103*, 2884–2886. (b) Gross, Z.; Nimri, S.; Barzilay, C. M.; Simkhovich, L. *J. Biol. Inorg. Chem.* **1997**, *2*, 492–506. (c) Hart-Davis, J.; Battioni, P.; Boucher, J. L.; Mansuy, D. *J. Am. Chem. Soc.* **1998**, *120*, 12524–12530. (d) Goh, Y. M.; Nam, W. *Inorg. Chem.* **1999**, *38*, 914–920. (e) Matsu-ura, M.; Tani, F.; Nakayama, S.; Nakamura, N.; Naruta, Y. *Angew. Chem., Int. Ed.* **2000**, *39*, 1989–1991. (f) McLain, J. L.; Lee, J.; Groves, J. T. *Biomimetic Oxidations Catalyzed by Transition Metal Complexes*; Meunier, B. Ed.; Imperial College Press: London, 2000; pp 91−169. (g) Watanabe, Y. *The Porphyrin Handbook*; Kadish, K. M., Smith, K. M., Guilard, R. Eds; Academic: New York, 2000; Vol. *4*, pp 97−117. (h) Ogliaro, F.; de Visser, S. P.; Cohen, S.; Sharma, P. K.; Shaik, S. *J. Am. Chem. Soc.* **2002**, *124*, 2806–2817. (i) Nam, W. *Comprehensive Coordination Chemistry II: From Biology to Nanotechnology*; Que, L., Jr., Tolman, W. T. Eds.; Elsevier Ltd.: Oxford, 2004; Vol. *8*, pp 281−307. (j) Crestoni, M. E.; Fornarini, S. *Inorg. Chem.* **2005**, *44*, 5379–5387.

10.1021/ic8013706 CCC: $40.75
Published on Web 09/13/2008

Scheme 1. The Rebound Mechanism for Mn(por)-Catalyzed C−H Oxidation (Square Box = Vacancy)

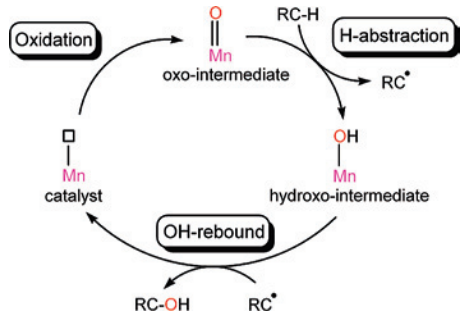

proposed for Mn[12] and Fe.[13] The rebound mechanism consists of (1) oxidation of the Mn^{III}(por) (por = porphyrin) catalyst to $Mn^{V}O$(por), (2) H atom abstraction from the substrate C–H bond, leading to an organic radical and a $Mn^{IV}OH$(por) intermediate, and (3) OH-rebound by OH transfer to the organic radical.

The key intermediate that initiates C−H hydroxylation in the rebound mechanism is $Mn^{V}O$(por), analogous to the $Fe^{IV}O$(por) postulated for cytochrome P450.[14] $Mn^{V}O$(por) compounds were first isolated and spectroscopically characterized by Groves and co-workers.[15,16] This pioneering work was extended by Nam and co-workers[17] and Newcomb and co-workers.[18] Other highly oxidized oxomanganese species have been studied in relation to biochemical systems, such as haloperoxides[19] and the oxygen-evolving complex of photosystem II.[20] Moreover, Mn(V) oxo complexes containing nonporphyrin ligands have also been characterized.[21]

Although experimental studies have established that the key intermediate contains the $Mn^{V}O$ group, the identity and even the presence of an additional axial ligand trans to the oxo is uncertain.[22] Very recently, Groves and co-workers found strongly pH-dependent O-transfer reactivity for $Mn^{V}O$(TMP) (TMP = tetramesitylporphyrin).[23] At a high pH, with bases like $^{t}Bu_4NOH$, the oxo complex is unreactive, whereas at a low pH, with acids like CH_3COOH, O transfer takes place. This behavior can be associated with acid−base equilibria involving three protonation states of the $Mn^{V}O$ system (Scheme 2), $[MnO(por)(H_2O)]^{+}$, MnO(por)(OH), and $[MnO_2(por)]^{-}$, the latter being the first known example of a *trans*-dioxomanganese compound.[23,24] Each of these species contains a different O-bound ligand trans to the oxo group and is thus likely to have different reactivity. De Angelis and co-workers showed that the increased reactivity by protonation in oxygen transfer to bromide is associated

(4) (a) Ozaki, S. I.; Roach, M. P.; Matsui, T.; Watanabe, Y. *Acc. Chem. Res.* **2001**, *34*, 818–825. (b) Poulos, T. L.; Li, H. Y.; Raman, C. S.; Schuller, D. J. *Adv. Inorg. Chem.* **2001**, *51*, 243–293. (c) Groves, J. T. *Proc. Natl. Acad. Sci. U. S. A.* **2003**, *100*, 3569–3574. (d) Matsunaga, I.; Shir, Y. *Curr. Opin. Chem. Biol.* **2004**, *8*, 127–132. (e) Meunier, B.; de Visser, S. P.; Shaik, S. *Chem. Rev.* **2004**, *104*, 3947–3980. (f) Ortiz de Montellano, P. R. *Cytochrome P450: Structure, Mechanism, and Biochemistry*, 3rd ed.; Kluwer Academic/Plenum Publishers: New York, 2005. (g) Denisov, I. G.; Makris, T. M.; Sligar, S. G.; Schlichting, I. *Chem. Rev.* **2005**, *105*, 2253–2278.

(5) (a) Groves, J. T. *J. Inorg. Biochem.* **2006**, *100*, 434–447. (b) Spiro, T. G.; Czernuszewicz, R. S.; Li, X. Y. *Coord. Chem. Rev.* **1990**, *100*, 541–571.

(6) (a) Hill, C. L.; Schardt, B. C. *J. Am. Chem. Soc.* **1980**, *102*, 6374–6375. (b) Mansuy, D. *Coord. Chem. Rev.* **1993**, *125*, 129–141.

(7) (a) Groves, J. T. *J. Chem. Educ.* **1985**, *62*, 928–931. (b) Groves, J. T. *J. Porphyrins Phthalocyanines* **2000**, *4*, 350–352.

(8) Balcells, D.; Raynaud, C.; Crabtree, R. H.; Eisenstein, O. *Chem. Commun.* **2008**, 744–746.

(9) Slaughter, L. M.; Collman, J. P.; Eberspacher, T. A.; Brauman, J. I. *Inorg. Chem.* **2004**, *43*, 5198–5204.

(10) (a) Groves, J. T.; McClusky, G. A. *J. Am. Chem. Soc.* **1976**, *98*, 859–861. (b) Ogliaro, F.; Harris, N.; Cohen, S.; Filatov, M.; de Visser, S. P.; Shaik, S. *J. Am. Chem. Soc.* **2000**, *122*, 8977–8989. (c) Bathelt, C. M.; Ridder, L.; Mulholland, A. J.; Harvey, J. N. *J. Am. Chem. Soc.* **2003**, *125*, 15004–15005. (d) Kumar, D.; de Visser, S. P.; Shaik, S. *J. Am. Chem. Soc.* **2003**, *125*, 13024–13025. (e) Bathelt, C. M.; Ridder, L.; Mulholland, A. J.; Harvey, J. N. *Org. Biomol. Chem.* **2004**, *2*, 2998–3005. (f) Shoneboom, J. C.; Cohen, S.; Lin, H.; Shaik, S.; Thiel, W. *J. Am. Chem. Soc.* **2004**, *126*, 4017–4034. (g) Shaik, S.; Kumar, D.; de Visser, S. P.; Altun, A.; Thiel, W. *Chem. Rev.* **2005**, *105*, 2279–2328. (h) Zurek, J.; Foloppe, N.; Harvey, J. N.; Mulholland, A. J. *Org. Biomol. Chem.* **2006**, *4*, 3931–3937. (i) Altun, A.; Shaik, S.; Thiel, W. *J. Am. Chem. Soc.* **2007**, *129*, 8978–8987. (j) Silaghi-Dumitrescu, R. *J. Biol. Inorg. Chem.* **2004**, *9*, 471–476. (k) Shaik, S.; Kumar, D.; de Visser, S. P. *J. Am. Chem. Soc.* **2008**, *130*, 10128–10140.

(11) (a) Sharma, P. K.; de Visser, S. P.; Ogliaro, F.; Shaik, S. *J. Am. Chem. Soc.* **2003**, *125*, 2291–2300. (b) Dhuri, S. N.; Seo, M. S.; Lee, Y.-M.; Hirao, H.; Wang, Y.; Nam, W.; Shaik, S. *Angew. Chem., Int. Ed.* **2008**, *47*, 3356–3359.

(12) Strassner, T.; Houk, K. N. *J. Am. Chem. Soc.* **2000**, *122*, 7821–7822.

(13) Collman, J. P.; Chien, A. S.; Eberspacher, T. A.; Brauman, J. I. *J. Am. Chem. Soc.* **1998**, *120*, 425–426.

(14) (a) Derat, E.; Shaik, S. *J. Am. Chem. Soc.* **2006**, *128*, 8185–8198. (b) Han, A. R.; Jeong, Y. J.; Kang, Y.; Lee, J. Y.; Seo, M. S.; Nam, W. *Chem. Commun.* **2008**, 1076–1078.

(15) Groves, J. T.; Lee, J.; Marla, S. S. *J. Am. Chem. Soc.* **1997**, *119*, 6269–6273.

(16) Jin, N.; Groves, J. T. *J. Am. Chem. Soc.* **1999**, *121*, 2923–2924.

(17) Nam, W.; Kim, I.; Lim, M. H.; Choi, H. J.; Lee, J. S.; Jang, H. G. *Chem.—Eur. J.* **2002**, *8*, 2067–2071.

(18) (a) Zhang, R.; Newcomb, M. *J. Am. Chem. Soc.* **2003**, *125*, 12418–12419. (b) Zhang, R.; Horner, J. H.; Newcomb, M. *J. Am. Chem. Soc.* **2005**, *127*, 6573–6582.

(19) (a) Lahaye, D.; Groves, J. T. *J. Inorg. Biochem.* **2007**, *101*, 1786–1797. (b) Jin, N.; Bourassa, J. L.; Tizio, S. C.; Groves, J. T. *Angew. Chem., Int. Ed.* **2000**, *39*, 3849–3851.

(20) (a) Pecoraro, V. L.; Hsieh, W. Y. *Inorg. Chem.* **2008**, *47*, 1765–1778. (b) Yano, J.; Robblee, J.; Pushkar, Y.; Marcus, M. A.; Bendix, J.; Workman, J. M.; Collins, T. J.; Solomon, E. I.; George, S. D.; Yachandra, V. K. *J. Am. Chem. Soc.* **2007**, *129*, 12989–13000. (c) Shimazaki, Y.; Nagano, T.; Takesue, H.; Ye, B.-H.; Tani, F.; Naruta, Y. *Angew. Chem., Int. Ed.* **2004**, *43*, 98–100. (d) Naruta, Y.; Maruyama, K. *J. Am. Chem. Soc.* **1991**, *113*, 3595–3596. (e) Limburg, J.; Vrettos, J. S.; Liable-Sands, L. M.; Rheingold, A. L.; Crabtree, R. H.; Brudvig, G. W. *Science* **1999**, *283*, 1524–1527. (f) Limburg, J.; Vrettos, J. S.; Chen, H. Y.; de Paula, J. C.; Crabtree, R. H.; Brudvig, G. W. *J. Am. Chem. Soc.* **2001**, *123*, 423–430.

(21) (a) Nehru, K.; Kim, S. J.; Kim, I. Y.; Seo, M. S.; Kim, Y.; Kim, S. J.; Kim, J.; Nam, W. *Chem. Commun.* **2007**, 4623–4625. (b) Mandimutsira, B. S.; Ramdhanie, B.; Todd, R. C.; Wang, H.; Zareba, A. A.; Czernuszewicz, R. S.; Goldberg, D. P. *J. Am. Chem. Soc.* **2002**, *124*, 15170–15171. (c) Wang, S. H.; Mandimutsira, B. S.; Todd, R.; Ramdhanie, B.; Fox, J. P.; Goldberg, D. P. *J. Am. Chem. Soc.* **2004**, *126*, 18–19. (d) Golubkov, G.; Bendix, J.; Gray, H. B.; Mahammed, A.; Goldberg, I.; Dibilio, A. J.; Gross, Z. *Angew. Chem., Int. Ed.* **2001**, *40*, 2132–2134. (e) Gross, Z.; Golubkov, G.; Simkhovich, L. *Angew. Chem., Int. Ed.* **2000**, *39*, 4045–4047. (f) Zhang, R.; Harischandra, D. N.; Newcomb, M. *Chem.—Eur. J.* **2005**, *11*, 5713–5720. (g) Workman, J. M.; Powell, R. D.; Procyk, A. D.; Collins, T. J.; Bocian, D. F. *Inorg. Chem.* **1992**, *31*, 1548–1550. (h) Collins, T. J.; Powell, R. D.; Slebodnick, C.; Uffelman, E. S. *J. Am. Chem. Soc.* **1990**, *112*, 899–901. (i) Collins, T. J.; Gordon-Wylie, S. W. *J. Am. Chem. Soc.* **1989**, *111*, 4511–4513. (j) MacDonnell, F. M.; Fackler, N. L. P.; Stern, C.; O'Halloran, T. V. *J. Am. Chem. Soc.* **1994**, *116*, 7431–7432.

(22) Song, W. J.; Seo, M. S.; George, S. D.; Ohta, T.; Song, R.; Kang, M.-J.; Tosha, T.; Kitagawa, T.; Solomon, E. I.; Nam, W. *J. Am. Chem. Soc.* **2007**, *129*, 1268–1277.

(23) Jin, N.; Ibrahim, M.; Spiro, T. G.; Groves, J. T. *J. Am. Chem. Soc.* **2007**, *129*, 12416–12417.

(24) Gross, Z. *Angew. Chem., Int. Ed.* **2008**, *47*, 2737–2739.

Scheme 2. Acid−Base Equilibria Involving the $[MnO(por)(X)]^+$ (X = H_2O, OH^-, and O^{2-}) Species

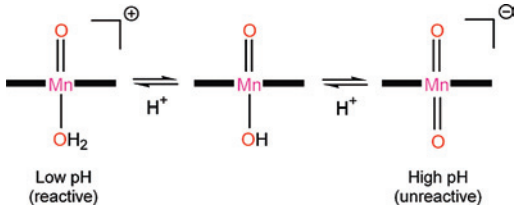

with the reduction of the low-spin/high-spin energy gap.[25] The critical role of the axial ligand has been well established for FeO−porphyrin systems.[26]

The spin state can strongly influence the reactivity of metal complexes.[10,27] This is the basis of the two-state reactivity model proposed by Shaik for cytochrome P450.[28] Very recently, we reported a computational density functional theory (DFT) study on the rebound mechanism for the oxidation of toluene by MnO(tHp)(X) (tHp = tetrahydrogenporphyrin), with X = Cl^-.[8] The calculations showed that both the H-abstraction and OH-rebound steps have low barriers and are exothermic (see Scheme 3), supporting the rebound mechanism for this reaction. The energy barrier of H abstraction is higher than that of OH rebound. This study also showed that the MnO(por)(Cl) intermediate has three possible spin states, a low-spin singlet state, a high-spin triplet state, and a high-spin quintet state. These spin states all occur within an energy span of only *ca.* 10 kcal mol^{-1}, and hence they are all thermally accessible. The Mn=O group requires radical oxyl character for efficient homolytic C−H cleavage, but the singlet state, having no oxyl character, is unreactive. In principle, singlet oxo complexes could also be reactive by transfer to the high-spin potential energy surface, if this surface is easily accessible. The oxyl character increases with the total spin of the system, and both the triplet and quintet states undergo H abstraction with very low energy barriers of *ca.* 2−4 kcal mol^{-1}. Although the oxyl character of the triplet is low, it is sufficient to promote H abstraction. Mayer and Gardner have shown that even diamagnetic oxo groups can have some activity for H-atom abstraction via proton-coupled electron transfer,[29] but the long times and high temperatures needed in this case compared to the very fast reaction occurring at room temperature suggest that a reagent with oxyl character is significantly more reactive.

Scheme 3. Energy Profile (kcal mol^{-1}) for the Rebound Mechanism in MnO(tHp)(Cl)-Catalyzed Toluene Oxidation, from ref 8[a]

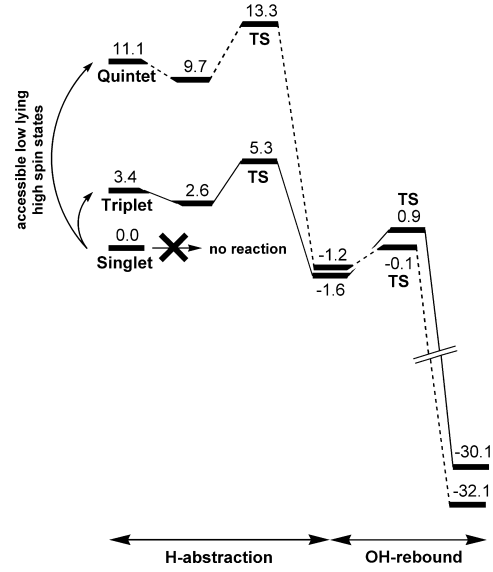

[a] The solid and dashed lines denote triplet and quintet states respectively.

Although this work provided mechanistic insight into the rebound mechanism for oxo-Mn^V−porphyrin complexes, only MnO(tHp)(Cl) was considered, so the critical role of the axial ligand remained unclear. Here, we present an extended study of toluene hydroxylation by $[MnO(por)(X)]^+$, with X = H_2O, OH^-, and O^{2-}. The electronic structure, stability, and reactivity of the different spin states are explored, and the axial ligand effect is discussed, helping to clarify the origin of the experimental results of Groves and co-workers.[23] A detailed molecular orbital analysis on the unprecedented *trans*-dioxomanganese species is also presented.

Oxyl character elongates Mn=O bonds, so it might be thought that higher trans-influence ligands (H_2O < OH^- < O^{2-}) should elongate the trans-Mn=O bond and thus enhance both oxyl character and reactivity. In fact, the opposite is true—the weakest trans-influence X = H_2O case shows the highest reactivity. We now show that this is because the higher trans-influence X ligands increase the low-spin−high-spin energy gap, leading to a slower reaction. These results are consistent with the experimental requirement for acidic pH found by Groves and co-workers[23] because this prevents deprotonation of the low trans-influence X = H_2O ligand.

Computational Details

Unrestricted DFT calculations were carried out using the BP86 functional.[30] Two different basis sets, I and II, were used. Basis set I (Stuttgart-Bonn scalar relativistic ECP with associated basis sets[31] for Mn and Cl and the all-electron 6-31G[32] for O, N, C, and

(25) De Angelis, F.; Jin, N.; Car, R.; Groves, J. T. *Inorg. Chem.* **2006**, *45*, 4268–4276.
(26) (a) Gross, Z.; Nimri, S. *Inorg. Chem.* **1994**, *33*, 1731–1732. (b) Hirao, H.; Que, L.; Nam, W.; Shaik, S. *Chem.—Eur. J.* **2008**, *14*, 1740–1756. (c) Sastri, C. V.; Park, M. J.; Ohta, T.; Jackson, T. A.; Stubna, A.; Seo, M. S.; Lee, J.; Kim, J.; Kitagawa, T.; Munck, E.; Que, L.; Nam, W. *J. Am. Chem. Soc.* **2005**, *127*, 12494–12495. (d) Nam, W.; Jin, S. W.; Lim, M. H.; Ryu, J. Y.; Kim, C. *Inorg. Chem.* **2002**, *41*, 3647–3652. (e) Urano, Y.; Higuchi, T.; Hirobe, M.; Nagano, T. *J. Am. Chem. Soc.* **1997**, *119*, 12008–12009. (f) Wang, R.; de Visser, S. P. *J. Inorg. Biochem.* **2007**, *101*, 1464–1472. (g) de Visser, S. P. *J. Biol. Inorg. Chem.* **2006**, *11*, 168–178.
(27) (a) Harvey, J. N.; Poli, R.; Smith, K. M. *Coord. Chem. Rev.* **2003**, *238*, 347–361. (b) Poli, R.; Harvey, J. N. *Chem. Soc. Rev.* **2003**, *32*, 1–8. (c) Poli, R. *Acc. Chem. Res.* **1997**, *30*, 494–501. (d) Poli, R. *Chem. Rev.* **1996**, *96*, 2135–2204.
(28) (a) Harris, N.; Cohen, S.; Filatov, M.; Ogliaro, F.; Shaik, S. *Angew. Chem., Int. Ed.* **2000**, *39*, 2003–2007. (b) Schroder, D.; Shaik, S.; Schwarz, H. *Acc. Chem. Res.* **2000**, *33*, 139–145. (c) Shaik, S.; Filatov, M.; Schroder, D.; Schwarz, H. *Chem.—Eur. J.* **1998**, *4*, 193–199.
(29) Gardner, K. A.; Mayer, J. M. *Science* **1995**, *269*, 1849–1851.
(30) (a) Perdew, J. P. *Phys. Rev. B: Condens. Matter Mater. Phys.* **1986**, *33*, 8822–8824. (b) Perdew, J. P. *Phys. Rev. B: Condens. Matter Mater. Phys.* **1986**, *34*, 7406. (c) Becke, A. *Phys. Rev. A: At., Mol., Opt. Phys.* **1988**, *38*, 3098–3100.
(31) (a) Andrae, D.; Haüssermann, U.; Dolg, M.; Stoll, H.; Preuss, H. *Theor. Chim. Acta* **1990**, *77*, 123–141. (b) Bergner, A.; Dolg, M.; Küchle, W.; Stoll, H.; Preuss, H. *Mol. Phys.* **1993**, *80*, 1431–1441.

Scheme 4. Model Reactants

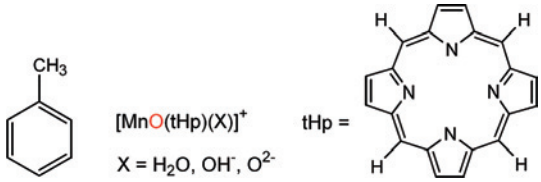

H) was used to optimize the geometries, and basis set II (the same as I but with added polarization functions[33] on all atoms) was used to refine the energies of the stationary points through single-point calculations. Geometry optimizations were carried out without any symmetry constraints. The geometries were fully optimized for each X ligand and each spin state. The nature of all stationary points was confirmed by an analytical calculation of frequencies. Each transition state was relaxed toward reactants and products using the vibrational data to confirm its nature. All energies given in the text are potential energies obtained with basis set II. Spin densities were evaluated by means of the natural population analysis approach,[34] using basis set II. All calculations were carried out with Gaussian 03.[35] This DFT methodology has been previously successfully applied by us in the study of toluene hydroxylation by MnO(por)(Cl).[8] Similar DFT methods have been also successfully used in the study of Mn-catalyzed olefin epoxidation.[36]

The catalytic system was simplified in order to reduce the computational cost (Scheme 4). The substituents of the porphyrin ligand were replaced by hydrogens, leading to the model tHp (tetrahydrogenporphyrin) ligand. Toluene was considered as a model substrate, and three different axial ligands (X = H_2O, OH^-, and O^{2-}), trans to the oxo group, were considered.

The rebound step of the mechanism (Scheme 1) was characterized for X = OH^- in the triplet state at the basis set II level, which showed that the energy profile is very similar to that of X = Cl^- (Scheme 3);[8] that is, the energy barrier of H abstraction is higher than that of OH rebound. Solvent effects were modeled by means of single-point calculations with the conductor-like polarizable continuum model method[37] considering acetonitrile as the solvent at the basis set II level. The presence of negatively charged species (X = O^{2-}) prompted the introduction of diffuse 6-31++G(d,p) functions[38] through single-point calculations. The introduction of either solvent effects or diffuse functions did not alter the gas-phase energy profiles at the basis set II level to any great extent. The results of all these calculations are given with more detail in the Supporting Information.

(32) Hehre, W. J.; Ditchfield, R.; Pople, J. A. *J. Phys. Chem.* **1972**, *56*, 2257–2261.
(33) (a) Ehlers, A. W.; Böhme, M.; Dapprich, S.; Gobbi, A.; Höllwarth, A.; Jonas, V.; Köhler, K. F.; Stegmann, R.; Veldkamp, A.; Frenking, G. *Chem. Phys. Lett.* **1993**, *208*, 111–114. (b) Höllwarth, A.; Böhme, H.; Dapprich, S.; Ehlers, A. W.; Gobbi, A.; Jonas, V.; Köhler, K. F.; Stegmann, R.; Veldkamp, A.; Frenking, G. *Chem. Phys. Lett.* **1993**, *203*, 237–240. (c) Hariharan, P. C.; Pople, J. A. *Theor. Chim. Acta* **1973**, *28*, 213–222.
(34) Reed, A. E.; Curtiss, L. A.; Weinhold, F. *Chem. Rev.* **1988**, *88*, 899–926.
(35) Frisch, M. J. et al. *GAUSSIAN 03*, revision D.01; Gaussian, Inc.: Wallingford, CT, 2004.
(36) (a) Abashkin, Y. G.; Collins, J. R.; Burt, S. K. *Inorg. Chem.* **2001**, *40*, 4040–4048. (b) Cavallo, L.; Jacobsen, H. *Inorg. Chem.* **2004**, *43*, 2175–2182. (c) Sears, J. S.; Sherrill, C. D. *J. Chem. Phys.* **2006**, *124*, 144314.
(37) Barone, V.; Cossi, M. *J. Phys. Chem. A* **1998**, *102*, 1995–2001.
(38) Clark, T.; Chandrasekhar, J.; Spitznagel, G. W.; Schleyer, P. V. *J. Comput. Chem.* **1983**, *4*, 294–301.

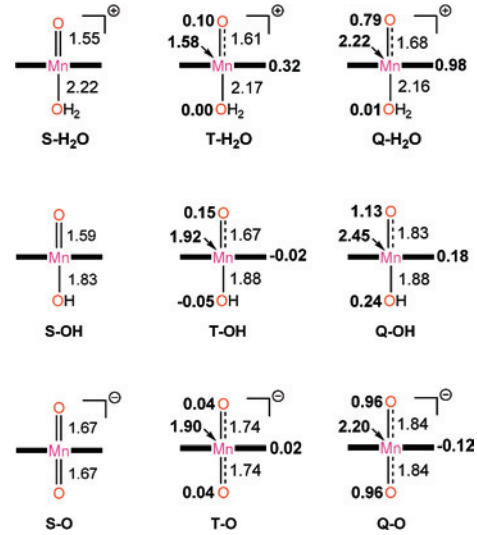

Figure 1. Manganese−oxygen bond distances in Ångstroms and local spin densities (bold) for $[MnO(por)(X)]^+$ (X = H_2O, OH^-, and O^{2-}).

Results

Structure and Spin of the Oxo Intermediates. Three different spin states, the singlet, triplet, and quintet, were computed for $[MnO(tHp)(H_2O)]^+$, predominant in acidic conditions (Figure 1). The main change is the Mn=O distance, which elongates with the total spin of the system: 1.55 Å in the singlet, **S-H_2O**; 1.61 Å in the triplet, **T-H_2O**; and 1.68 Å in the quintet, **Q-H_2O**. The Mn−O elongation is compensated by shortening of the trans Mn−OH_2 bond from 2.22 Å in **S−H_2O** to 2.17 Å and 2.16 Å in **T-H_2O** and **Q-H_2O**, respectively.

The geometry of the neutral species, MnO(tHp)(OH), was also optimized for the three spin states (Figure 1). Regardless of the spin state, the Mn=O distances are longer than those found for $[MnO(tHp)(H_2O)]^+$, owing to the stronger trans influence of the OH axial ligand. As in the case of X = H_2O, the Mn=O distance elongates as the total spin of the system increases, from 1.59 Å in **S-OH** to 1.83 Å in **Q-OH**. Interestingly, this Mn=O bond elongation is no longer compensated by a shortening of the trans Mn−OH bond, which instead elongates, from 1.83 Å in the singlet to 1.88 Å in the two high-spin states.

The Mn=O bond distances of the *trans*-dioxo species, $[MnO_2(tHp)]^-$ (Figure 1), are longer than the Mn=O distances of $[MnO(tHp)(H_2O)]^+$ and MnO(tHp)(OH), owing to the much higher trans influence of the oxo ligand versus H_2O and OH^-. As the spin state of the system increases, the Mn=O bonds again become longer: 1.67 Å in **S-O**, increasing to 1.74 Å in **T-O**, and to 1.84 Å in **Q-O**.

The local spin densities of $[MnO(tHp)(H_2O)]^+$ were computed for the triplet and quintet states (Figure 1). In **T-H_2O**, most of the spin is concentrated on the metal, with Mn having a local spin density of 1.58. Interestingly, the apical oxygen of the water ligand has no spin density, whereas the oxo oxygen has a small spin density of 0.10, meaning that **T-H_2O** has oxyl character. The rest of the spin density, 0.32, is delocalized over the porphyrin. In **Q-H_2O**, the local spin density on manganese, 2.22, is even higher.

Table 1. Relative Energies of the Different Spin States for Each Axial X Ligand in Kilocalories Per Mole

X	singlet	triplet	quintet
H_2O	0.0	4.7	12.1
OH^-	0.0	9.2	22.4
O^{2-}	0.0	27.3	39.1

The spin density on the porphyrin also increases, in this case to 0.98. The oxyl character also intensifies since the spin density on the oxo group, 0.79, is much higher than in the triplet. Only the apical oxygen of the aqua ligand remains unaffected, with an almost null spin density of 0.01.

The local spin densities of MnO(tHp)(OH) are also given in Figure 1. The triplet state has almost null spin densities on the OH (−0.05) and porphyrin (−0.02) ligands, and most of the spin is localized on manganese (1.92). Both **T-OH** and **Q-OH** have oxyl character, as shown by the spin densities on the oxo group, 0.15 and 1.13, respectively, which also indicates that, as in $[MnO(tHp)(H_2O)]^+$, the oxyl character is much higher in the quintet than in the triplet. The oxygen atom of the axial OH ligand has significant spin density only in **Q-OH** (0.24).

The spin density of $[MnO_2(tHp)]^-$ was also analyzed (Figure 1). In this case, the local spin density on the porphyrin remains almost null in the triplet (0.02) and quintet (−0.12) states. In both **T-O** and **Q-O**, a spin density of *ca.* 2.00 is associated with the metal. The local spin densities on the oxygen atoms are very low in the triplet (0.04), pointing to low oxyl character. In contrast, the oxyl character is much stronger in the quintet state, with local spin densities of 0.96 on both oxygens.

The geometries of the **S-H_2O**, **S-OH**, and **S-O** complexes show the strong trans influence of the axial ligand. The Mn−X distance shortens from 2.22 Å, for X = H_2O, to 1.67 Å, for X = O^{2-}, whereas the Mn═O distance elongates from 1.55 Å to 1.67 Å. Thus, as the π-donor character of X increases, the Mn−X bond becomes stronger and the trans Mn═O bond becomes weaker. The same trend applies for the triplet and quintet states. The nature of the axial ligand also has an influence on the Mn−tHp bond. The maximum value of the Mn−N−N−N dihedral angle is 0.0° in **S-O**, 3.9° in **S-OH**, and 12.4° in **S-H_2O**. The out-of-plane displacement of Mn with respect to the four-nitrogen centroid of the porphyrin was 0.0 Å (**S-O**), 0.10 Å (**S-OH**), and 0.26 Å (**S-H_2O**). The trans influence of X decreases from X = O^{2-} to X = H_2O, accompanied by a motion of the metal center out of the tHp plane away from X.

With the singlet ground state always assigned zero energy, the triplet and quintet states of $[MnO(tHp)(H_2O)]^+$ are found at 4.7 and 12.1 kcal mol^{-1}, respectively (see Table 1). For MnO(tHp)(OH), they are at 9.2 (triplet) and 22.4 (quintet) kcal mol^{-1}, and for $[MnO_2(tHp)]^-$, they are at 27.3 (triplet) and 39.1 (quintet) kcal mol.$^{-1}$ Hence, the energy ordering is always singlet below triplet below quintet, regardless of the axial ligand. Nevertheless, the axial ligand has a strong influence on the energy gap between the singlet and the high-spin states. This gap becomes significantly wider as the trans influence and π-donor character of the axial ligand increase from X = H_2O through OH^- to O^{2-}. For instance, the

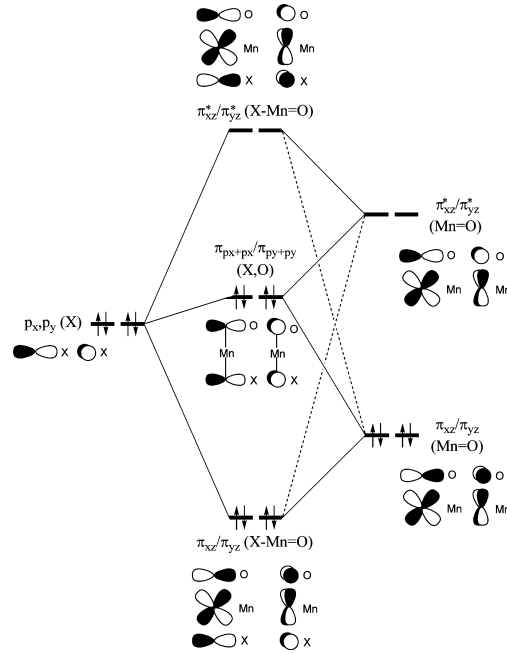

Figure 2. Schematic interaction diagram for the π(X−Mn−O) molecular orbitals, shown for X = O^{2-}.

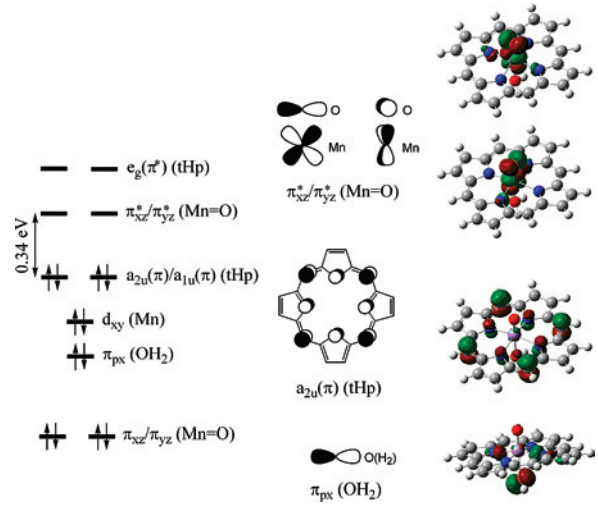

Figure 3. Molecular orbitals for the singlet state of $[MnO(tHp)(H_2O)]^+$.

singlet−triplet energy gap increases from 4.7 kcal mol^{-1}, for X = H_2O, to 9.2 kcal mol^{-1}, for X = OH^-, and to 27.3 kcal mol^{-1}, for X = O^{2-}. This trend has also been observed by Ghosh and co-workers[39] and by De Angelis and co-workers,[25] in similar $Mn^VO(por)(X)$ systems (X = H_2O, OH^-, and O^{2-}). Similar spin patterns with multiple possible spin states[40] have been found in Mn-catalyzed epoxidation.[36]

Electronic Structure of the Oxo Intermediates. The electronic structures of **S-H_2O**, **S-OH**, and **S-O** can be understood in molecular orbital terms (Figures 2−5). Regardless of the axial ligand, the d_{z^2}, $d_{x^2-y^2}$, d_{xz}, and d_{yz} atomic orbitals of Mn are involved in bonding molecular orbitals.

(39) (a) Ghosh, A.; Gonzalez, E. *Isr. J. Chem.* **2000**, *40*, 1–8. (b) Ghosh, A.; Vangberg, T.; Gonzalez, E.; Taylor, P. *J. Porphyrins Phthalocyanines* **2001**, *5*, 345–356. (c) Ghosh, A.; Taylor, P. R. *Curr. Opin. Chem. Biol.* **2003**, *7*, 113–124.

(40) de Visser, S. P.; Ogliaro, F.; Gross, Z.; Shaik, S. *Chem.—Eur. J.* **2001**, *7*, 4954–4960.

The d_{z^2} makes a σ bond with the p_z orbitals of the oxo group and the axial ligand, while the $d_{x^2-y^2}$ is involved in a σ bond with the lone pair of the porphyrin nitrogens. These bonding orbitals, mostly centered on either O or N, are well below the frontier level. Closer to the frontier, we find the π bonding orbitals associated with the X−Mn═O fragment, which involve the d_{xz} and d_{yz} orbitals. The fifth d metal orbital, d_{xy}, remains as a nonbonding doubly occupied orbital, close to the frontier level. Thus, to the extent such assignments are meaningful, the metal center in **S-H$_2$O**, **S-OH**, and **S-O** can be formulated as d^2-Mn(V) in all three cases.

To describe the electronic structure of the X−Mn═O moiety, we consider the interaction of Mn═O and the axial ligand, X. Figure 2 shows this interaction diagram for X = O^{2-}. The π bond of Mn═O is represented by the bonding π_{xz} ($d_{xz} + p_x$) and π_{yz} ($d_{yz} + p_y$) and the antibonding π_{xz}* ($d_{xz} - p_x$) and π_{yz}* ($d_{yz} - p_y$) orbitals. The axial ligand participates to the Mn═O π bonding with two lone pairs, p_x and p_y, lying in energy between the π(Mn═O) and π*(Mn═O) levels. Combining the π(Mn═O) orbitals with the X lone pairs leads to all in-phase orbitals, π_{xz} (X−Mn═O) and π_{yz}(X−Mn═O). A second set of molecular orbitals, higher in energy, arises from the mixing of the X lone pairs with both π(Mn═O) and π*(Mn═O). These orbitals can be formulated as p(X) − π(Mn═O) + π*(Mn═O). The relative weight of π(Mn═O) and π*(Mn═O) depends on the energy level of p(X). When p(X) has high energy, the contribution of π*(Mn═O) is important. In the X = O^{2-} case, this combination yields the nonbonding π_{px+px} and π_{py+py} orbitals represented in Figure 2. Finally, the highest-energy combination corresponds to the all out-of-phase π_{xz}*(X−Mn═O) and π_{yz}*(X−Mn═O) orbitals. This interaction diagram is also qualitatively valid for X = H_2O and OH^-.

The double degenerate set of four-electron−three-orbital interactions represented in Figure 2 transfers electron density from X to π*(Mn═O) and weakens the MnO bond. Where this interaction is very weak, such as for X = H_2O, the transfer is negligeable and the MnO bond is very short and best described as a triple Mn≡O bond. Where the interaction between X and π*(Mn═O) increases (X = OH^-), the transfer of electron density is larger and the MnO bond lengthens. At the extreme case (X = O^{2-}), the participation of π*(Mn═O) is maximal, and the MnO bond significantly lengthens. Thus, although there is always a degenerate set of π-type orbitals for describing the two manganese−oxygen bonds, in the case of X = O^{2-}, each of them is best viewed as a double Mn═O bond.

For **S-H$_2$O** (Figure 3), the highest occupied molecular orbitals (HOMOs) are two π orbitals of the porphyrin ligand, a_{1u} (given in the Supporting Information) and a_{2u}, which are doubly occupied and have the same energy, located above that of the doubly occupied Mn d_{xy} orbital. The lowest unoccupied molecular orbitals (LUMOs) are two degenerate π*(Mn═O) orbitals (π_{xz}* and π_{yz}*). Interestingly, the axial aqua ligand does not mix with the π(Mn═O) and π*(Mn═O) orbitals. In this case, the lone pair of water, π_{px}, is far removed in energy from the π*(Mn═O) orbital and does not overlap with the manganese orbitals. If one ignores the deeper orbitals mostly centered on O and N and having σ Mn−ligand character, the electronic configuration of **S-H$_2$O** can be described as $(\pi_{xz})^2(\pi_{yz})^2(\pi_{px})^2(d_{xy})^2(a_{2u})^2(a_{1u})^2$. **S-H$_2$O** has a small HOMO−LUMO gap of only 0.34 eV.

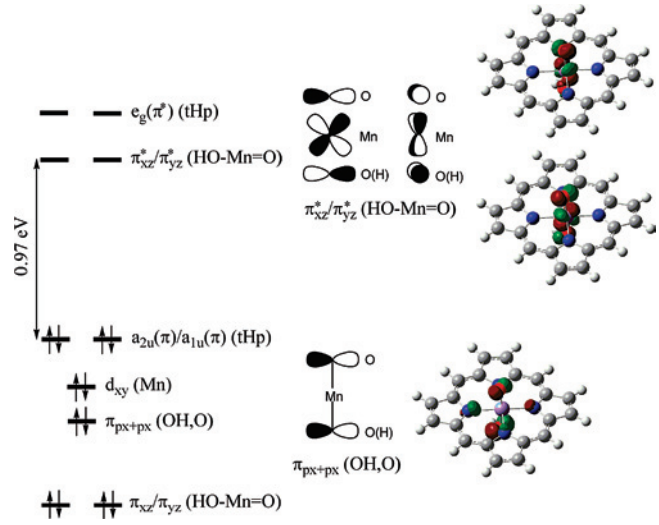

Figure 4. Molecular orbitals for the singlet state of MnO(tHp)(OH).

The electronic configuration of **T-H$_2$O** is described as $(\pi_{xz})^2(\pi_{yz})^2(\pi_{px})^2(a_{2u})^2(a_{1u})^2(d_{xy})^1(\pi_{xz}^*)^1$, which means that one electron is promoted from the d_{xy} Mn orbital and not from the porphyrin despite the energy ordering of the molecular orbitals in the singlet state. The configuration of the quintet state, **Q-H$_2$O**, is $(\pi_{xz})^2(\pi_{yz})^2(\pi_{px})^2(a_{1u})^2(d_{xy})^1(a_{2u})^1(\pi_{xz}^*)^1(\pi_{xz}^*)^1$. These data suggest that the high spin states of $[MnO(tHp)(H_2O)]^+$ are generated by promoting one electron from the metal d_{xy} orbital to the π*(Mn═O) orbitals.[41] The population of the antibonding π*(Mn═O) orbitals accounts for the elongation of the Mn═O bond and the oxyl character found in the high-spin states (Figure 1). In the case of **Q-H$_2$O**, one additional electron is promoted from the $a_{2u}(\pi)$ orbital of the porphyrin to a π*(Mn═O) orbital. Since the π*(Mn═O) orbital is mostly centered on the metal, the manganese spin density is always higher than that on the oxygen (Figure 1). The two bonding π(Mn═O) orbitals remain doubly occupied in both **T-H$_2$O** and **Q-H$_2$O**.

The molecular orbital structure of **S-OH** is very similar to that of **S-H$_2$O** (Figure 4). Two degenerate π orbitals of the porphyrin, a_{1u} and a_{2u}, lie at the frontier energy level, and immediately below in energy is the doubly occupied Mn d_{xy} orbital. The bonding π_{xz} and π_{yz} orbitals remain much deeper in energy. In between the π_{xz}, π_{yz}, and d_{xy} levels there is a nonbonding combination of the p_x lone pairs of the apical oxygens (π_{px+px}). In this case, the lone pairs of X = OH^- are more diffuse and closer in energy to π*(Mn═O), which favors the overlap with the metal d orbitals. As a consequence, the axial OH ligand participates in the π orbitals of the HO−Mn═O moiety (Figure 4) and thus raises the energy of the all out-of-phase combinations, π_{xz}*(HO−Mn═O) and

(41) Contrary to what was said in ref 8, the d_{xy} orbital of manganese is half-occupied in both the triplet and quintet states of MnO(tHp)(Cl). Using the same notation as in the article, the electron configurations of the singlet, triplet, and quintet states are $(\pi_{xz})^2(\pi_{yz})^2(d_{xy})^2(\pi_{px})^2(\pi_{py})^2(a_{1u})^2(a_{2u})^2$, $(\pi_{xz})^2(\pi_{yz})^2(\pi_{px})^2(\pi_{py})^2(a_{1u})^2(a_{2u})^2(d_{xy})^1(\pi_{xz}^*)^1$, and $(\pi_{xz})^2(\pi_{yz})^2(\pi_{px})^2(\pi_{py})^2(a_{1u})^2(d_{xy})^1(a_{2u})^1(\pi_{xz}^*)^1(\pi_{xz}^*)^1$, respectively.

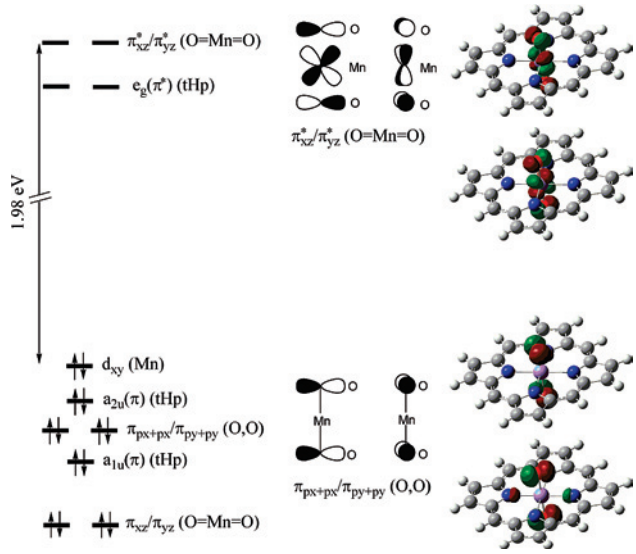

Figure 5. Molecular orbitals for the singlet state of $[MnO_2(tHp)]^-$.

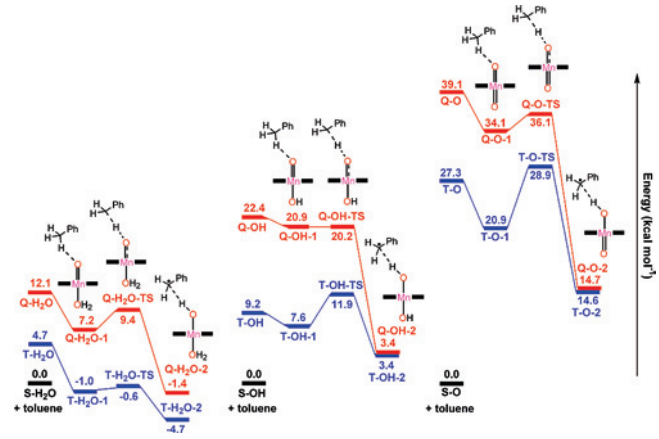

Figure 6. Hydrogen-abstraction energy profiles for X = H_2O (left), OH^- (center), and O^{2-} (right). The black, blue, and red profiles correspond to the singlet, triplet, and quintet states, respectively.

π_{yz}*(HO−Mn═O). As a result, compared to **S-H$_2$O**, **S-OH** has a wider HOMO−LUMO energy gap of 0.97 eV. Ignoring the deeper energy levels, the electronic configuration of **S-OH** can be described as $(\pi_{xz})^2(\pi_{yz})^2(\pi_{px+px})^2(d_{xy})^2(a_{2u})^2(a_{1u})$.[2]

The orbital analysis of **T-OH** and **Q-OH** shows that the electronic configurations of these species are $(\pi_{xz})^2(\pi_{yz})^2(\pi_{px+px})^2(a_{2u})^2(a_{1u})^2(d_{xy})^1(\pi_{xz}^*)^1$ and $(\pi_{xz})^2(\pi_{yz})^2(a_{2u})^2(a_{1u})^2(\pi_{px+px})^1(d_{xy})^1(\pi_{xz}^*)^1(\pi_{yz}^*)^1$, respectively. Hence, as in the case of X = H_2O, the high-spin states are generated from the singlet by promoting one electron from the d_{xy} orbital of the metal to the π* orbitals of HO−Mn═O. In the case of the quintet, one electron is promoted from the nonbonding π_{px+px} orbital and not from the porphyrin. The presence of singly occupied π*(HO−Mn═O) orbitals in the high-spin states accounts for the oxyl character and the Mn═O bond elongation in **T-OH** and **Q-OH** (Figure 1). In addition, the participation of the axial OH ligand in these π* orbitals accounts for the oxyl character of the OH group as well as the elongation of the Mn−OH bond.

The electronic structure of $[MnO_2(tHp)]^-$ around the frontier level (Figure 5) is clearly different from that seen for MnO(tHp)(OH) and $[MnO(tHp)(H_2O)]^+$ (Figures 3 and 4). In this case, the HOMO is the doubly occupied metal d_{xy}. Next below comes the porphyrin π orbitals a_{2u} and a_{1u}, but not at the same energy as for X = H_2O and OH^-, and between these a pair of doubly occupied orbitals, π_{px+px} and π_{py+py}, consisting of nonbonding combinations of the p_x and p_y orbitals of the trans oxygens (Figure 5). As for X = H_2O and OH^-, the bonding π orbitals of X−Mn═O lie much deeper in energy, far below the frontier energy level. But in contrast, these π orbitals and their antibonding partners, π_{xz}* and π_{yz}* (Figure 5), have equal and thus larger contributions from both apical oxygens. In contrast with the X = OH^- case, the overlap between the metal d orbitals and the oxygen p orbitals is optimal. Indeed, these orbitals correspond to the whole trans-O═Mn═O moiety rather than just to Mn═O. The LUMO is the degenerate set of $e_g(\pi^*)$ orbitals of the porphyrin, while the LUMO+1 is the degenerate set of π*(O═Mn═O) orbitals. The energy gap between the HOMO and the π_{xz}* and π_{yz}* orbitals, 1.98 eV, is *ca.* twice as large as that of **S-OH** and *ca.* 6 times as large as that of **S-H$_2$O**. The electronic configuration of **S-O** can be described as $(\pi_{xz})^2(\pi_{yz})^2(a_{1u})^2(\pi_{px+px})^2(\pi_{py+py})^2(a_{2u})^2(d_{xy})^2$.

The electronic configurations of **T-O** and **Q-O** are $(\pi_{xz})^2(\pi_{yz})^2(a_{1u})^2(\pi_{px+px})^2(\pi_{py+py})^2(a_{2u})^2(d_{xy})^1(\pi_{xz}^*)^1$ and $(\pi_{xz})^2(\pi_{yz})^2(a_{1u})^2(\pi_{py+py})^2(a_{2u})^2(\pi_{px+px})^1(d_{xy})^1(\pi_{xz}^*)^1(\pi_{yz}^*)^1$, respectively. Hence, as for X = H_2O and X = OH^-, the π* orbitals associated with X−Mn═O become singly occupied in the high-spin states, which explains the weakening of this bond and the gain in oxyl character (Figure 1). In this case, the participation of both oxygens in the π_{xz}* and π_{yz}* orbitals explains that the elongation of the Mn═O bond and the delocalization of oxyl character affect the whole O═Mn═O fragment. The other singly occupied orbitals are d_{xy}, in **T-O**, and d_{xy} and π_{px+px}, in **Q-O**, which are doubly occupied in **S-O**. The high-spin states of $[MnO_2(tHp)]^-$ are thus generated by promoting electrons from the d_{xy} and π_{px+px} orbitals.

Reactivity of the Oxo Intermediates. The reactivity of $[MnO(tHp)(H_2O)]^+$, MnO(tHp)(OH), and $[MnO_2(tHp)]^-$ in the C−H oxidation of toluene was explored by computing the corresponding intermediates and transition states. To compare reactivity, we always take the singlet ground state as having zero energy (Figure 6). The reaction has two successive elementary steps: radical hydrogen abstraction followed by OH rebound (Scheme 1). Only radical H abstraction is analyzed in detail since H abstraction has by far the highest energy barrier for the closely related case of MnO(tHp)(Cl)[8] (Scheme 3). The fast subsequent OH-rebound step[42] is much more exothermic, and once the $PhCH_2$ radical has been generated, it collapses promptly to give the final product. This is also confirmed for X = OH^- in the triplet state (see the Supporting Information). In this case, the H-abstraction barrier (4.3 kcal mol^{-1}) is clearly higher than that of the OH rebound (0.4 kcal mol^{-1}). As in the case of MnO(tHp)(Cl), no H-abstraction transition state is found for the singlet states of any of the three Mn−oxo

(42) (a) Bowry, V. W.; Ingold, K. U. *J. Am. Chem. Soc.* **1991**, *113*, 5699–5707. (b) Atkinson, J. K.; Ingold, K. U. *Biochemistry* **1993**, *32*, 9209–9214. (c) Newcomb, M.; Letadic, M. H.; Putt, D. A.; Hollenberg, P. F. *J. Am. Chem. Soc.* **1995**, *117*, 3312–3313.

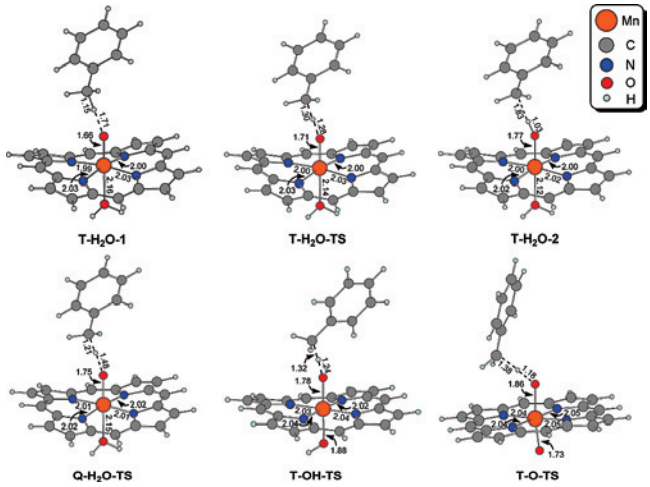

Figure 7. Optimized geometries of selected stationary points for toluene H-abstraction. See Figure 6 for notation.

complexes, regardless of X. None of these oxo species can therefore hydroxylate toluene in their singlet states. Indeed, some unreactive Mn(V)−oxo−porphyrin complexes have been characterized as stable, diamagnetic singlet compounds.[22,23] In contrast, both the triplet and quintet states undergo H abstraction. A similar effect of spin on reactivity has been also found in Mn-catalyzed olefin epoxidation.[43]

The triplet state of $[MnO(tHp)(H_2O)]^+$ interacts with toluene, giving rise to a prereaction complex, **T-H$_2$O-1**, lying 5.7 kcal mol^{-1} below **T-H$_2$O** + toluene (Figure 6). In this species, a benzylic C−H of the substrate and the oxo group of the catalyst are weakly bound through a C−H···O hydrogen bond, with a H···O distance of 1.71 Å (Figure 7). This intermediate undergoes radical H abstraction, yielding **T-H$_2$O-2** through the transition state **T-H$_2$O-TS**. The reaction is exothermic ($\Delta E = -3.7$ kcal mol^{-1}) and has a very low energy barrier of only 0.4 kcal mol^{-1}. This process consists of concerted cleavage of the benzylic C−H bond and the formation of a new O−H bond, as shown by the metric parameters. The C−H elongates from 1.15 Å in **T-H$_2$O-1** to 1.83 Å in **T-H$_2$O-2**, while the O−H shortens from 1.71 Å in **T-H$_2$O-1** to 1.03 Å in **T-H$_2$O-2**. At **T-H$_2$O-TS**, the C−H and O−H distances have intermediate values of 1.30 Å and 1.28 Å, respectively. The intermediate **T-H$_2$O-2** can be formulated as the hydroxo $[Mn(OH)(tHp)(H_2O)]^+$ complex bound to the $PhCH_2$ radical by a weak CH···O bond. The transformation of the Mn═O group into Mn−OH in **T-H$_2$O-1** → **T-H$_2$O-2** involves the elongation of the Mn−O bond, from 1.66 Å to 1.77 Å, accompanied by shortening of the trans Mn−OH_2 bond, from 2.16 Å to 2.12 Å. The bond between manganese and the tHp porphyrin is unaffected by the reaction, and the four Mn−N bond distances of *ca.* 2 Å (2.00−2.06 Å) do not undergo significant change along the reaction pathway.

The quintet state of $[MnO(tHp)(H_2O)]^+$ follows a reaction pathway analogous to that of **T-H$_2$O**. The **S-H$_2$O** → **Q-H$_2$O** transformation is followed by the formation of a moderately exothermic prereaction complex, **Q-H$_2$O-1**, with $\Delta E = -4.9$ kcal mol^{-1} (Figure 6). In **Q-H$_2$O-1**, toluene is bound to the oxo group through a weak CH···O hydrogen bond (d(CH···O) = 2.04 Å). In the C−H activation transition state, **Q-H$_2$O-TS** (Figure 7), C−H bond cleavage (d(C···H) = 1.21 Å) accompanies O−H bond formation (d(O···H) = 1.48 Å). The geometries of **T-H$_2$O-TS** and **Q-H$_2$O-TS** are very similar, the latter being more reactant-like. As in the triplet surface, the H transfer is exothermic ($\Delta E = -8.6$ kcal mol^{-1}) and has a low energy barrier ($\Delta E^{\ddagger} = 2.2$ kcal mol^{-1}). The transition state connects with **Q-H$_2$O-2**, an intermediate in which the $PhCH_2$ radical interacts with the MnOH fragment with a long C···H distance of 1.98 Å. The reaction pathway from **Q-H$_2$O-1** to **Q-H$_2$O-2** also involves the elongation of the Mn−O bond associated with the Mn═O → Mn−OH transformation, whereas the Mn−N bonds of the Mn(tHp) part remain unaffected. The whole quintet pathway lies above the triplet in energy.

The energy profiles for the C−H activation of toluene with MnO(tHp)(OH) and $[MnO_2(tHp)]^-$ were also computed. The structures of the stationary points and the change in the geometrical parameters are very similar to those for X = H_2O. Therefore, only the geometries of the triplet transition states, **T-OH-TS** and **T-O-TS**, are given in detail in Figure 7.

In the case of X = OH^-, the C−H oxidation is also preceded by the formation of an intermediate with a weak CH···O bond between the oxo complex and the substrate. This species is formed in both the triplet and quintet surfaces, with favorable albeit very small values of ΔE (−1.6 kcal mol^{-1} for **T-OH-1** and −1.5 kcal mol^{-1} for **Q-OH-1**; Figure 6). Both **T-OH-1** and **Q-OH-1** undergo H transfer from toluene to the oxo group, leading to **T-OH-2** and **Q-OH-2**, respectively. These reactions are exothermic and involve very low energy barriers;[44] for instance, on the triplet surface, ΔE is −4.2 kcal mol^{-1} and $\Delta E^{\ddagger}$ is 4.3 kcal mol^{-1}. In the triplet transition state, **T-OH-TS** (Figure 7), the formation of the new O−H bond and the cleavage of the benzylic C−H bond are concerted, as pointed to by the O···H and C···H distances of 1.24 Å and 1.32 Å, respectively. These distances are almost the same as those in **T-H$_2$O-TS**. In fact, the main geometrical differences between **T-H$_2$O-TS** and **T-OH-TS** are shown by the Mn−O bonds: in **T-OH-TS**, the Mn−O bond is longer and the axial Mn−O(H) bond is shorter, due to the higher coordination strength and trans effect of X = OH^- versus X = H_2O.

Toluene coordinates weakly with **T-O**, giving rise to intermediate **T-O-1**, in which a benzylic C−H makes a CH···O hydrogen bond with one of the oxo groups. This initial exothermic step ($\Delta E = -6.4$ kcal mol^{-1}; Figure 6) is followed by radical H abstraction, leading to **T-O-2**, which consists of the $PhCH_2$ radical weakly bound to the hydroxo group of Mn(OH)(tHp)(O). The H-abstraction step is exo-

(43) (a) Strassner, T.; Houk, K. N. *Org. Lett.* **1999**, *1*, 419–421. (b) Cavallo, L.; Jacobsen, H. *Eur. J. Inorg. Chem.* **2003**, *89*, 2–902. (c) Abashkin, Y. G.; Burt, S. K. *Org. Lett.* **2004**, *6*, 59–62.

(44) The energy barrier associated to **Q-OH-1** → **Q-OH-TS** in Figure 6 is −0.7 kcal mol^{-1}. This result is associated with the single-point calculations of the energies at the DZP (double-ζ + polarization; basis set II) level. The energies at the DZ (double-ζ without polarization; basis set I) level, at which the geometries were optimized, gave a reasonable energy barrier of 0.4 kcal mol^{-1}. These results clearly indicate that H abstraction has a very low energy barrier.

thermic ($\Delta E = -6.3$ kcal mol^{-1}) and has a low energy barrier ($\Delta E^{\ddagger} = 8.0$ kcal mol^{-1}). A benzylic hydrogen of toluene is transferred to an oxo group of $[MnO_2(tHp)]^-$ in the transition state, **T-O-TS** (Figure 7), as shown by the C···H (1.38 Å) and O···H (1.18 Å) distances. The reaction pathway on the quintet surface is analogous to that of the triplet, but with a lower energy barrier of 2.0 kcal mol^{-1} and a more exothermic result ($\Delta E = -19.4$ kcal mol^{-1}).

Discussion

The oxidation of bromide by the isomeric oxo-Mn(V)-2-TMPyP and oxo-Mn(V)-4-TMPyP (TMPyP = tetra-N-methylpyrydil porphyrin) complexes has been analyzed in a combined experimental/theoretical study by De Angelis and co-workers.[25] The unexpectedly higher reactivity of the more electron-rich 4-TMPyP isomer was attributed to the higher proton affinity and smaller singlet−quintet energy gap with respect to 2-TMPyP. Linear transit scan calculations of the potential energy surface along the Mn═O coordinate showed that both the singlet and triplet states are unreactive, whereas the quintet promotes oxo-transfer to Br^- through a low-energy barrier.

Our calculations, with all transition states fully characterized, show that only high-spin complexes promote H abstraction. Thus, in contrast to O transfer to bromide, triplet as well as quintet states of the manganese−oxo−porphyrin complexes are reactive, because they both have oxyl character. Even a small oxyl character permits H abstraction, as shown by the fact that the triplet and quintet states, which differ greatly in oxyl character, have similar barriers above their respective prereaction complexes. The key factor that dominates the reactivity, however, is the promotion energy from the unreactive singlet ground state to the higher spin states that permits reaction. Where this is small, as in X = H_2O, the reaction is fast.[23]

The DFT methodology is not able to rank different spin states when they are close in energy. Thus, the result that the ground states of all three complexes are singlet is most likely valid for larger low-spin−high-spin energy gaps (X = OH^- and O^{2-}). Indeed, the $[MnO_2(TMP)]^-$ (TMP = tetra-mesityl porphyrin) complex was characterized as a diamagnetic singlet species.[23] However, in the case of the aqua complex, where the triplet state is only 4.7 kcal mol^{-1} above the singlet, the reverse ordering of these states cannot be eliminated. Even with this limitation, our calculations clearly indicate that C−H oxidation is very facile for $[MnO(tHp)(H_2O)]^+$ and increasingly difficult for MnO(tHp)(OH) and $[MnO_2(tHp)]^-$. These results agree with experimental results: isolable complexes of the general formula MnO(TDCPP)(X) (TDCPP = tetra-(2,6-dichlorophenyl) porphyrin), in which the nature of X may be uncertain, were shown to be singlet diamagnetic species,[22] consistent with high-spin species being reactive. In agreement with our findings, O-transfer reactions were shown to be strongly pH-dependent and to prefer acid.[23] In such a case, the equilibrium of Scheme 2 is shifted toward the aqua complex, which is indeed calculated to be the most reactive.

The energy ordering found at our level of calculations, **S** < **T** < **Q**, arises from the promotion of electrons to the antibonding π^*(X−Mn═O) orbitals. Thus, the low-spin−high-spin energy gap is mainly determined by the energy of these orbitals. Axial X ligands with a high trans influence increase the energy of the π^*(X−Mn═O) orbitals, thus widening the **S/T** and **S/Q** energy gaps. The widening of the low-spin−high-spin energy gaps by increasing the trans influence has been also reported by De Angelis and co-workers for Mn-catalyzed bromide oxidation.[25]

Our results are counterintuitive in the sense that higher trans-influence X ligands might have been thought to elongate the trans Mn═O bonds and make them more reactive. Here, we show that the dominant factor is the large increase in the **S/T** and **S/Q** gaps caused by high trans-influence ligands. This entirely dominates the reactivity so that the lowest trans-influence X ligand, H_2O, now gives the highest reactivity.

The molecular orbital analysis of the singlet states reveals that the manganese d_{xy} orbital is doubly occupied in all systems, and therefore the metal center is formally Mn(V) in all cases. The high-spin states are generated by promoting electrons from the frontier orbitals of the MnO(tHp)(X) complexes. For all Xs, the π(Mn═O) orbitals are too deep in energy to be the source of electrons. The two high-spin states are generated by promoting electrons from the d_{xy}(Mn) orbital to π^*(X−Mn═O). In the case of the quintet state, an additional electron is promoted from either a porphyrin π orbital, a_{2u} in **Q-H$_2$O**,[25] or a nonbonding combination of the oxygen lone pairs, π_{px+px} in **Q-OH** and **Q-O**. In this manner, the axial ligand and the porphyrin ring both may play a role in the reactivity of the Mn═O bond.

Regardless of X, the singlet ground state is not able to hydroxylate toluene. These results suggest that the radical oxyl character found in the high-spin states is needed for C−H activation. In this case, the Mn−oxyl radical species react with toluene, generating the benzyl $PhCH_2$ radical. Even a small amount of oxyl character permits a low-energy barrier reaction; the triplet and quintet are both equally reactive even though the triplet has much lower oxyl character. The need for oxyl character is also crucial in the manganese-catalyzed oxidation of water[45] and in methane activation by $(Al_2O_3)_x^+$ ($x = 3, 4, 5$) clusters.[46]

Conclusions

The reactivity of $[MnO(por)(X)]^+$ (por = porphyrin; X = H_2O, OH^-, and O^{2-}) for H abstraction from toluene, the key step in C−H oxidation, has been analyzed with DFT calculations. Transition states have been identified for the reactive triplet (**T**) and quintet (**Q**) states of all complexes, while singlet (**S**) states are always unreactive. Oxyl character, found only in the triplet and quintet states, is thus essential for efficient C−H activation. The much smaller oxyl

(45) (a) Siegbahn, P. E. M.; Crabtree, R. H. *J. Am. Chem. Soc.* **1999**, *121*, 117–127. (b) Lundberg, M.; Blomberg, M. R. A.; Siegbahn, P. E. M. *Inorg. Chem.* **2004**, *43*, 264–274.

(46) Feyel, S.; Döbler, J.; Höckendorf, R.; Beyer, M. K.; Sauer, J.; Schwarz, H. *Angew. Chem., Int. Ed.* **2008**, *47*, 1946–1950.

character of the triplet is sufficient for high reactivity. We find that the lowest trans-influence X ligand, H_2O, gives the most reactive complex. This is counterintuitive because high trans-influence X ligands would be expected to elongate the Mn═O bond and increase the oxyl character, thus enhancing reactivity. Contrary to this expectation, but consistent with experimental results, we show that reactivity in fact increases along the series $X = O^{2-} < OH^- < H_2O$; that is, reactivity increases as the trans influence of X decreases. We find that the dominant effect of the higher trans-influence X ligands is the increase of the **S/T** and **S/Q** energy gaps that they cause, thus making attainment of the needed high-spin states harder. The higher reactivity at acidic pH is thus rationalized by the preference for having $[MnO(por)(H_2O)]^+$ over MnO(por)(OH) or $[MnO_2(por)]^-$.

Acknowledgment. D.B., C.R., and O.E. thank the CNRS, the Ministère de l'Enseignement Supérieur et de la Recherche, and the Institut Charles Gerhardt Montpellier for funding. D.B. thanks Sanofi-Aventis for a postdoctoral fellowship. R.H.C. thanks the NSF (Grant 0614403) for funding.

Supporting Information Available: Listings of optimized geometries of all stationary points reported in the article together with their potential energies (*E*) at the basis set II level and the full author list for ref 35. Complete energy profile for $X = OH^-$ in the triplet state, including the rebound step. H-abstraction energy profiles at the CPCM(acetonitrile)/basis set II level and introducing diffuse 6-31++G(d,p) functions. Plot of the a_{1u} molecular orbital. This material is available free of charge via the Internet at http://pubs.acs.org.

IC8013706